RSC Advances

PAPER

View Article Online
View Journal | View Issue

Check for updates

Cite this: *RSC Adv.*, 2025, **15**, 24256

Facile synthesis of a Ni–Cu composite reinforced with a *para*-phenylenediamine layer for enhanced hydrogen evolution reaction†

Soufiane Skakri,[a] Anas El Attar,[ab] Saad Benhaiba,[a] Badr Bouljoihel,‡[a] Abdellah Aaddane,[a] Anas Mouakkar,[a] Adiba Rais[a] and Mama El Rhazi*[a]

Received 11th April 2025
Accepted 15th June 2025

DOI: 10.1039/d5ra02533h

rsc.li/rsc-advances

In the race to develop new catalysts for water splitting, researchers are increasingly focusing on the design of cost-effective materials, particularly first-row transition metals. Nickel and copper catalysts are promising candidates due to their low cost and excellent compatibility. Herein, for the first time, the electrochemical synthesis of Ni–Cu-based nanomaterials reinforced with a *para*-phenylenediamine (*p*PD) layer for the HER is reported. A very simple method involving the electrodeposition of a *p*PD layer on a carbon paste electrode (CPE), followed by the electrodeposition of Ni–Cu particles at a constant current to form Ni_4Cu_1/*p*PD/CPE, was employed. The morphological, structural and electrochemical properties of the catalyst were thoroughly characterized using several techniques such as field-emission scanning electron microscopy (FE-SEM), X-ray diffraction (XRD), cyclic voltammetry (CV) and electrochemical impedance spectroscopy (EIS). The catalytic performance and stability of the catalyst were evaluated in a 1 M KOH solution using linear sweep voltammetry and chronoamperometry, respectively. The prepared Ni_4Cu_1/*p*PD/CPE electrocatalyst exhibited high activity toward HER in an alkaline medium, achieving a very low overpotential of −70 mV *vs.* RHE at 10 mA cm^{-2} and a value of 87 mV dec^{-1} for Tafel slope. The results indicate that the prepared Ni_4Cu_1/*p*PD/CPE electrocatalyst is a highly promising catalytic material for effective green hydrogen production.

Introduction

With the tremendous increase in the global population and the continuous advancement of various technologies, the worldwide demand for energy consumption has escalated, leading to a critical challenge in meeting human energy needs.[1] Currently, fossil fuels are the primary source of energy; however, their usage releases numerous pollutants into the environment and contributes to future challenges such as greenhouse gas emissions, CO_2 emissions, and global warming.[2] The development of clean energy technology, such as water splitting, has emerged as a promising strategy for producing green hydrogen.[3,4] The HER generally requires three stages in alkaline solutions.[5] The first is the Volmer reaction, also known as electrochemical hydrogen adsorption: $H_2O + M + e^- \rightarrow MH_{ads} + OH^-$. In this step, a water molecule dissociates, producing a hydroxide ion and hydrogen adsorbed on the catalyst surface. The second step is electrochemical desorption, or the Heyrovsky reaction, in which the hydrogen adsorbed during the Volmer step is discharged with an electron at the electrode–solution interface, leading to the formation of hydrogen gas (H_2). Finally, the third step is chemical desorption, known as the Tafel reaction, where two adsorbed hydrogen atoms formed during the Volmer step combine to produce hydrogen gas (H_2).[6]

Platinum is the most effective catalyst for the HER. However, its high cost and limited earth abundance nature affect the cost-effectiveness of HER technology.[7,8] To overcome this issue, many strategies have been investigated using first-row transition metals such as nickel, copper and cobalt.[9–11] Nickel-based catalysts have garnered significant interest and have been thoroughly investigated. However, the activity and durability of Ni-based catalysts remain unsatisfactory. Recent research on synthetic Ni-based alloys has demonstrated that the nickel content in the alloy has a significant impact on both the alloy's morphological characteristics and electrochemical properties.[12,13] On the other hand, copper is an inexpensive, nonprecious transition metal with a face-centered cubic structure and lattice characteristics comparable to those of nickel. It has been reported that alloying nickel with copper exhibits favorable

[a]*Laboratory of Materials, Membranes, and Environment, Faculty of Sciences and Technologies Mohammedia, University Hassan II of Casablanca, Morocco. E-mail: Mama.elrhazi@fstm.ac.ma*

[b]*Centrale Lille, UMET–Unité Matériaux et Transformation, UMR 8207, F-59000 Lille, France*

† Electronic supplementary information (ESI) available. See DOI: https://doi.org/10.1039/d5ra02533h

‡ Dr Badr Bouljoihel, who made significant contributions to the development of this work, sadly passed away before the submission of this manuscript. He was a brilliant scientist, and the authors gratefully acknowledge his insight, dedication, and lasting impact on this research.

synergistic effects and good electrocatalytic properties toward HER with an overpotential of 140 mV at 10 mA cm^{-2}; meanwhile, the corresponding Tafel slope was 79 mV dec^{-1}.[14] However, the synthesis method requires a significant amount of time. Hüner *et al.* succeeded in depositing Ni–Cu on 3D printed electrodes, enhancing their kinetic activity. The combination of Pd nanoparticles with nickel–copper foam leads to a special fractal structure with a high surface area and a very low overpotential towards HER.[15,16]

One of the most advantageous approaches to improving the catalytic performance of catalysts is to combine them with conducting polymers, as reported recently by many authors.[17–20] This combination provides a large specific surface area, strong electrical conductivity, and excellent stability under alkaline conditions. This approach has already been used in many studies for the oxidation of alcohol (ethanol oxidation reaction EOR and methanol oxidation reaction MOR) using different conducting polymers, such as polyaniline,[21] polypyrrole,[22] poly-*para*-phenylenediamine,[23] and poly-*ortho*-phenylenediamine, as support of bimetallic nanoparticles.[24] The presence of polyaniline as a supporting matrix ensures a homogeneous distribution of the deposited palladium–silver nanoparticles, leading to excellent electrocatalytic activity and higher resistance to intermediate catalyst species.[25] Furthermore, Zhanzhao Li and coworkers elaborated a MoS_2/rGO/PPD/O-MWCNT catalyst *via* a hydrothermal process at 220 °C for 24 h, and they investigated the effect of *para*-phenylenediamine on the HER of the MoS_2/rGO/PPD/O-MWCNT catalyst. The presence of *p*PD ensures good catalytic activity with 47.6 mA cm^{-2} as current density at an overpotential of 200 mV. This is mainly due to the fast electron transfer during the electrocatalytic reaction, coupled with a large surface area providing numerous active sites.[26] Park *et al.* synthesized a catalyst *via* a solvothermal process at 120 °C for 72 h and studied the effect of amine-based COF on the HER performance of the catalyst. It was concluded that the introduction of *p*-phenylenediamine and 2-nitro-*p*-phenylenediamine enhances the performance of the catalysts due to the modification of the electrocatalytic properties by increasing the proton transfer at the electrode–solution interface.[27] Ji and coworkers prepared different catalysts with metal cobalt nanoparticles and different phenylenediamines (*o*-phenylenediamine, *m*-phenylenediamine, *p*-phenylenediamine) *via* pyrolysis at 900 °C for 2 h in N_2 at 5 °C min^{-1} to investigate HER and OER. The catalyst Co@OPDBS exhibited a remarkable performance for both cathodic HER and anodic OER reactions, which was assigned to the highest charge-transfer kinetics, conversion efficiency and exposed more active sites with an overpotential η_{10} of 172 mV and 289 mV, respectively.[28] However, these studies suffer from serious drawbacks, such as the time-consuming synthesis process and high temperature. These aspects increase the cost of catalyst preparation and limit its widespread use in large-scale applications.[29,30]

To the best of our knowledge, this is the first report on the combination of *para*-phenylenediamine as a support matrix and Ni–Cu-based composite using an electrochemical synthesis approach to enhance the electrocatalytic performance of HER. Herein, a detailed investigation of the electrodeposition of *para*-phenylenediamine, copper and nickel particles was conducted using two simple pot synthesis methods. In order to achieve this purpose, our electrocatalysts were electro-synthesized in two steps using a single batch of potassium chloride solution containing copper and nickel chloride and another batch containing an appropriate concentration of *para*-phenylenediamine in sulfuric acid. The electrodeposition mode of *para*-phenylenediamine was investigated using cyclic voltammetry, chronoamperometry and chronopotentiometry. Galvanostatic and potentiostatic modes were applied to allow the deposition of nickel–copper particles. We carefully examined parameters that could affect the deposition process, including the salt concentration, deposition time, and deposition mode. The electrochemical behavior and stability of our catalyst towards HER were investigated using linear sweep voltammetry (LSV), electrochemical impedance spectroscopy (EIS), cyclic voltammetry (CV) and chronopotentiometry (CP) methods. The acquired results show that our electrocatalysts exhibit good durability, long stability, and good catalytic activity under alkaline conditions.

Experimental

Compounds and chemicals

Graphite (powder, <20 μm, synthetic, 100%) (MW = 12), H_2SO_4 (36%) (MW = 98), (*para*-phenylenediamine) (*p*PD) (99%) (MW = 108.14), mineral oil (heavy) (99%), $CuCl_2$, $2H_2O$ (99%) (MW = 170.48), $NiCl_2$, $6H_2O$ (97%) (MW = 237.69), potassium ferri/ferrocyanide $K_3Fe(CN)_6/K_4Fe(CN)_6$ $3H_2O$ (ACS reagent >99%), potassium chloride (KCl, extra pure, >99%) (MW = 74.55), and potassium hydroxide (KOH, 85%) (MW = 56.11) were provided by Sigma-Aldrich. All other chemicals were of analytical reagent grade and were used as received.

Preparation of the modified electrodes

A carbon paste electrode was prepared by mixing graphite powder (1 g) and paraffin oil (300 μl) in a mortar until a homogeneous paste was formed, which was then packed into the Teflon tube electrode (3 mm) cavity (CPE).[31–33] The electrochemical deposition of *para*-phenylenediamine was performed in a solution containing the monomer (5 mM of *p*PD in 1 M of H_2SO_4), followed by the galvanostatic electrodeposition of Ni–Cu within a solution containing $NiCl_2$ and $CuCl_2$ in 0.5 M of KCl with different salt concentrations. The electrode was named Ni_4Cu_1/*p*PD/CPE.

Synthesis of modified carbon paste electrode using *para*-phenylenediamine

The synthesis of poly *para*-phenylenediamine (*p*PD) was carried out *via* cyclic voltammetry using a three-electrode system. A carbon paste electrode, a platinum wire, and an Ag/AgCl electrode was used as working, auxiliary, and reference electrodes, respectively. First, the *p*PD monomer (5.10^{-3} M) was dissolved in 1 M H_2SO_4 solution, followed by electrodeposition on the CPE for 15 cycles in a potential range between −0.3 and 0.9 V *vs.* Ag/AgCl at a scan rate of 0.05 V s^{-1}. Two other approaches were used to synthesize the (*p*PD), which comprises galvanostatic and potentiostatic modes. The as-prepared *p*PD/CPE electrodes were used for electrodeposition of nickel–copper particles.

Fabrication of nickel–copper particles

It is important to indicate that the deposition mechanism is a significant factor in the determination of the shape of the bimetallic particles on the electrode.[34,35] The as-prepared *p*PD/CPE electrodes were carefully washed with bi-distilled water and placed in another aqueous solution containing 0.2 M $NiCl_2$–0.05 M $CuCl_2$ in 0.5 M KCl (the ratio 4/1 was already optimized in our previous work[35]). Two approaches have been investigated to prepare the Ni_4Cu_1 particles: the galvanostatic mode (applying a constant current density) and the potentiostatic mode (the applied potential of the prepared electrode was taken from the galvanostatic curve). Fig. 1 summarizes the fabrication procedures of the Ni_4Cu_1/*p*PD/CPE electrocatalyst.

Characterization and electrochemical measurements

SEM imaging was performed using a field-emission scanning electron microscope (HITACHI SU8220) at an accelerating voltage of 10 kV. The morphologies and compositions were further investigated using an energy-dispersive X-ray (EDX) detector coupled to FEG-SEM with an EDX detector (Oxford) and Transmission Electron Microscope (TEM) (acceleration voltage 200 kV, source: field emission gun, resolution 0.12 nm in imaging mode). XRD patterns were obtained by a Bruker D8-Advance X-ray diffractometer with Cu Kα irradiation ($\lambda = 1.541874$ A).

All electrochemical measurements were controlled with the Versa-Studio software and conducted using the VersaSTAT 4 system in a typical three-electrode configuration with the modified electrode as the working electrode, a silver chloride electrode Ag/AgCl as the reference electrode, and a platinum disc as the auxiliary electrode. All recorded potentials were adjusted to the reversible hydrogen electrode according to the following equation: $E_{RHE} = E_{Ag/AgCL} + 0.197V + 0.059$ pH.[36] The catalytic performance of our modified electrode (electrocatalyst) was evaluated using linear sweep voltammetry from 0.1 to −0.6 (V *vs.* RHE) at a scan rate of 0.005 V s^{-1}.[37] Tafel plots were extracted from LSV curves using the equation: $\eta = b\log(j) + a$ (η: overpotential, *j*: current density, *b*: Tafel slope, *a*: Tafel constant).[38] The electrochemical active surface area (ECSA) was calculated by the double layer capacitance method, and the charge transfer electron was determined by electrochemical impedance spectroscopy (EIS).

Results and discussion

Effect of electrodeposition modes on *p*PD

The effect of the electrodeposition mode was investigated using three different electrodeposition modes on *p*PD on the CPE electrode. The first experiment was conducted using cyclic voltammetry (CV) from −0.3 to 0.9 at a scan rate of 0.05 V s^{-1} using 15 cycles (Fig. S1a†). Notably, the monomer oxidation occurs at 0.6 V *vs.* Ag/AgCl during the first cycle, while we can observe that in the backward scan, two reduction peaks appear at 0.27 and 0.45 V *vs.* Ag/AgCl, in line with the previous findings obtained by Halim *et al.*[39] It's worth mentioning that the current of the

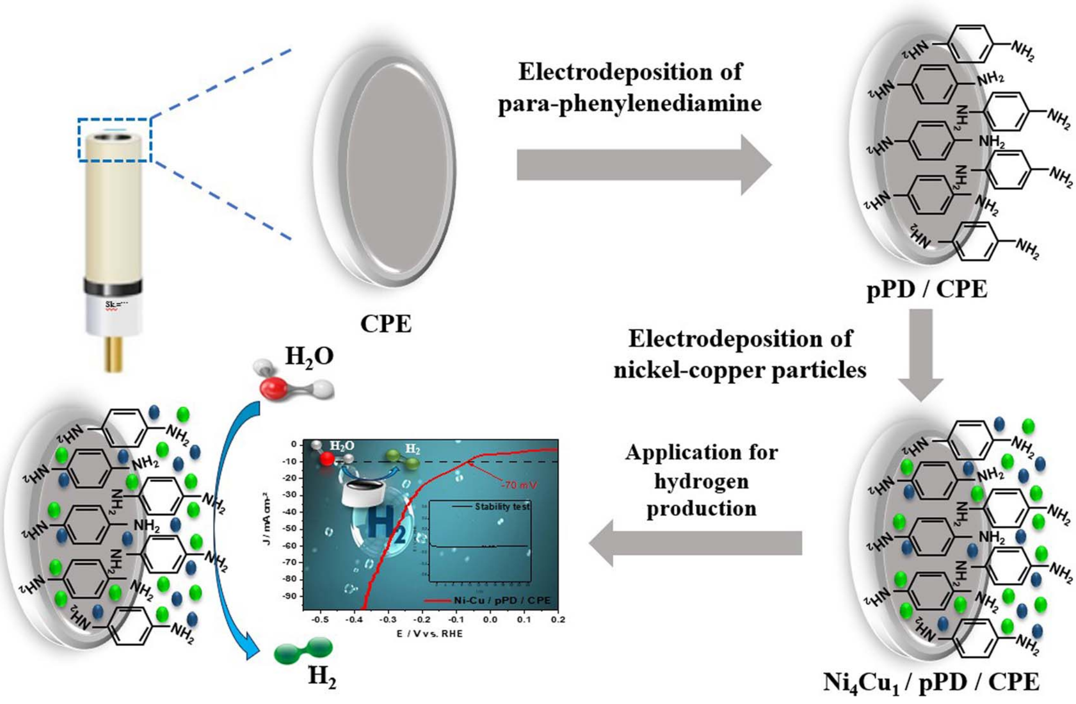

Fig. 1 Schematic of the fabrication steps of the Ni_4Cu_1/*p*PD/CPE electrocatalyst and its application for the HER in alkaline media.

cathodic and anodic peaks of the polymer increased with the consecutive potential cycling, indicating the formation of an electroactive layer of the polymer.[40] The second electrode was prepared using the galvanostatic mode (CP) at a current of 0.1 mA for 40 s. As shown in Fig. S1b,† the potential increased instantly during the first seconds and then stabilized at 1.45 V, demonstrating that the *p*PD film was successfully synthesized.[41] The last experiment was conducted using the chronoamperometry (CA) method at 0.7 V for 40 s (Fig. S1c†). According to the potentiostatic curve, the electrodeposition process comprises two steps. During the first step, the current increases (t < 3 s), indicating the formation of a radical cation. The current then decreased from 110 μA to 30 μA for 40 s, which was due to the deposition of the poly-*p*PD film.[42]

After the modification with poly-*p*PD, the electrode was placed in a solution containing 200 mM $NiCl_2$ and 50 mM $CuCl_2$ prepared in 0.5 M KCl and a current of −3 mA was applied for 150 s. Fig. 2a shows the galvanostatic deposition curves of the as-prepared electrodes. During the first second, the potential decreases rapidly for the three electrocatalysts until a value of −0.95 V/*vs.* Ag/AgCl, indicating the reduction of nickel–copper cations on the electrode surface. Then, between 20 and 150 s, the potential gradually increased with time, attributed to the formation of hydrogen bubbles on the Ni–Cu particles.[43]

To evaluate the catalytic efficiency of the as-prepared electrodes, the electrocatalytic response in 1 M KOH was investigated by LSV (Fig. 2b). The LSV curves reveal that the deposition of *p*PD with cyclic voltammetry $(CPE/pPD)_{CV}$ exhibits poor HER activity compared to the galvanostatic mode $(CPE/pPD)_{CP}$ and the potentiostatic mode $(CPE/pPD)_{CA}$, with an overpotential η_{10} of −503 mV, which might be as a result of a polymer layer formation on the surface of the electrode, which limits its conductivity and consequently reduces its active sites and performance. In contrast, the use of the galvanostatic mode $(CPE/pPD)_{CP}$ and the potentiostatic mode $(CPE/pPD)_{CA}$ demonstrates better electrocatalytic activity with an overpotential η_{10} of −206 mV and −245 mV, respectively. It should be noted that with the enhancement in overpotential (−275 mV>), the $(CPE/pPD)_{CA}$ exhibits higher electrocatalytic performance toward HER than $(CPE/pPD)_{CP}$. For $(CPE/pPD)_{CA}$, the higher activity toward HER is clearly due to the good conductivity of *p*PD deposited by the potentiostatic mode, as demonstrated in previous reported experiments.[26,27] SEM images of Ni_4Cu_1 particles deposited on *p*PD by CV methods $(CPE/pPD)_{CV}$, and by potentiostatic method $(CPE/pPD)_{CA}$ are shown in Fig. S3.† The electrocatalyst prepared with *p*PD by potentiostatic deposition (Fig. S3a and b†) reveals the presence of a smooth surface with a slice-shaped which provides a significant surface area. While the electrocatalyst prepared with *p*PD by the CV

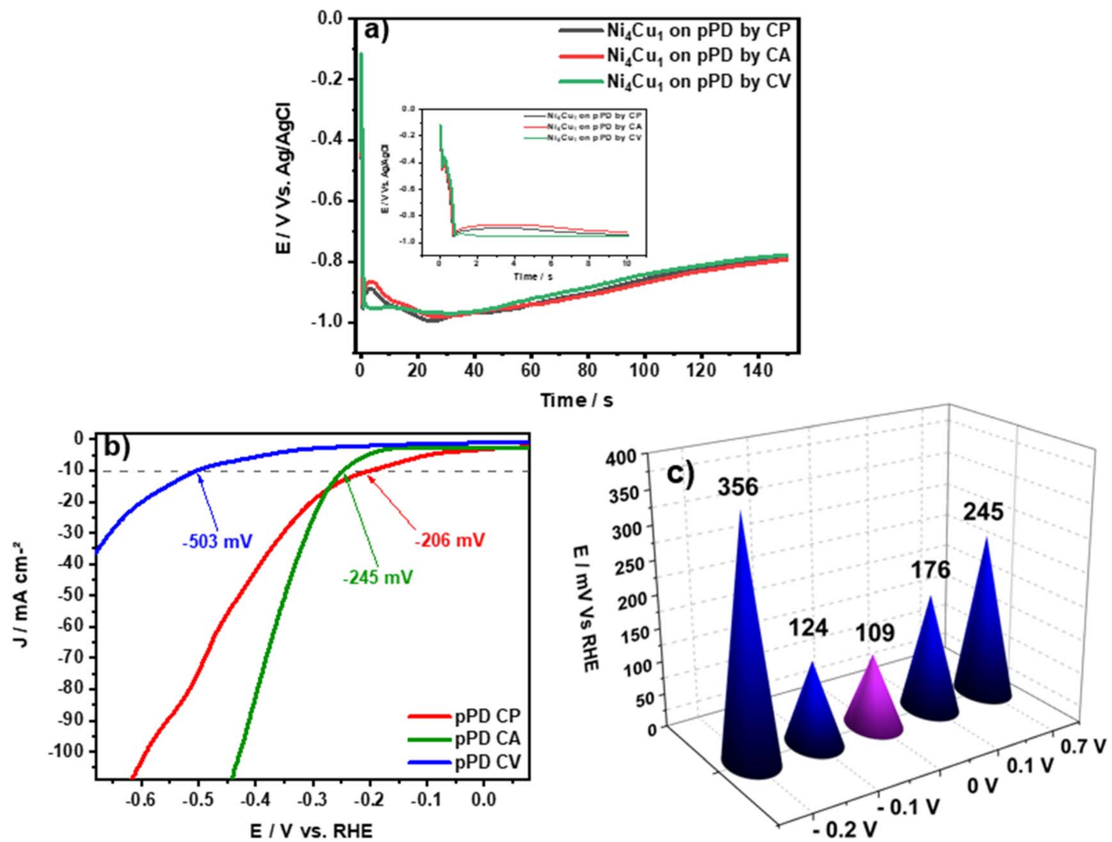

Fig. 2 (a) Chronopotentiometry curves of the galvanostatic deposition of Ni_4Cu_1 on the *p*PD deposit on CPE by different electrodeposition modes. (b) LSV curves of Ni_4Cu_1/*p*PD/CPE using three different electrodeposition modes of *para*-phenylenediamine (*p*PD). (c) Outcomes of the LSV test in 1 M KOH showing different overpotentials at 10 mV cm^{-2} for the prepared electrodes in 1 M KOH solution at different electrodeposition potentials of *para*-phenylenediamine.

method (Fig. S3c and d†) shows a good distribution of Ni–Cu particles on the electrode, it may be noted that the particles are flower-shaped. Since reducing the overpotential is the primary challenge in HER,[44] the effect of the deposition potential of *p*PD was investigated in order to determine the most suitable deposition potential to generate a higher amount of hydrogen. The electrocatalytic response of the different electrodes is shown in Fig. 2c; the lowest overpotential η_{10} (−109 mV) was obtained at an applied potential of 0 V. *vs.* Ag/AgCl, while the recording overpotential for the applied potentials −0.2, −0.1, 0.1, and 0.7 V were −356, −124, −176, and −245 mV, respectively. The higher catalytic efficiency of the prepared electrocatalyst at 0 V *vs.* Ag/AgCl toward HER may be related to the fact that the deposition of the *p*PD on the surface of the electrode by a simple adsorption of the monomer onto the electrode surface, which provides a large number of active sites for the nickel–copper deposition. It is important to highlight that the surface state plays an important role before the deposition of the bimetallic particle, as mentioned by many authors.[34]

Effect of the electrodeposition mode of nickel–copper particles

Once the electrodeposition mode of the *para*-phenylenediamine has been optimized, and to incorporate nickel–copper on the surface of the as-prepared electrode $(CPE/pPD)_{CA}$, the next step is to find the appropriate deposition mode of the Ni_4Cu_1 particles. To this end, the behavior of our catalyst will be investigated using two different electrodeposition techniques, galvanostatic mode and potentiostatic mode. Fig. S4a† shows a chronopotentiometry curve of the deposition of Ni–Cu at −3 mA for 150 s. The potential decreases rapidly to a more negative value from −0.4 V to −0.9 V *vs.* Ag/AgCl, and represents the reduction of nickel–copper cations on the electrode surface. The potential stabilizes after 10 s at −0.9 (V *vs.* Ag/AgCl), reaching a plateau, probably due to the evolution of hydrogen on the crystallites of the Ni–Cu particles, as reported by Chemchoub *et al.*[45] The second approach involved the potentiostatic deposition of Ni–Cu particles by applying a constant potential of −0.9 V *vs.* Ag/AgCl for 150 s (Fig. S4b†). The chronoamperometry curve shows that the potential increases and stabilizes after 25 s, indicating the nucleation of the nickel–copper particles. The same behavior for nickel cobalt particles was reported by indicating 3D nucleation.[46] The growth of nickel–copper particles and their activity toward HER were examined in 1 M KOH. Fig. 3a shows the results obtained using the two approaches explained above. It can be noticed that a low overpotential η_{10} of −109 mV was recorded using galvanostatic mode, while an overpotential of −205 mV was observed using potentiostatic mode. A potential shift of −96 mV was observed between the two methods. Subsequent investigations will be conducted under galvanostatic conditions.

The mass of nickel–copper particles deposited on the electrode ($(CPE/pPD)_{CA}$) related to different electrodeposition currents was studied (the current was varied from −0.75 mA to

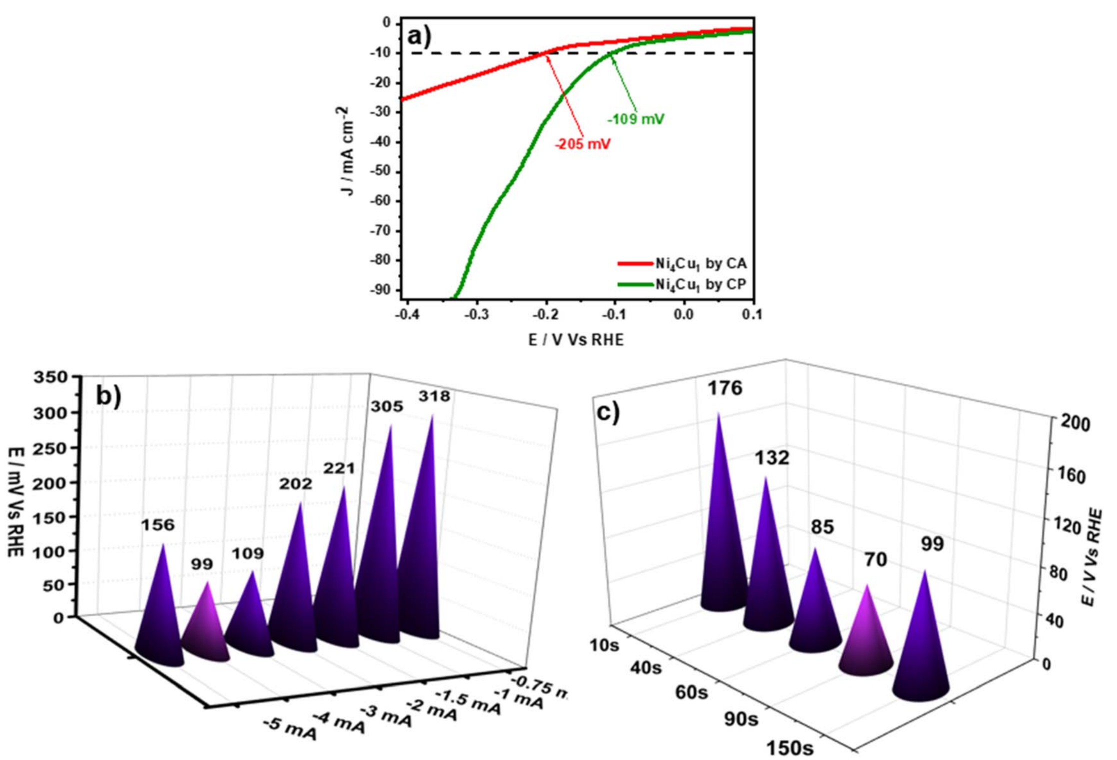

Fig. 3 (a) LSV curve of Ni_4Cu_1 particle electrodeposition after the deposition of *para*-phenylenediamine using two different approaches. The galvanostatic mode (green), the potentiostatic mode (red), (b and c) outcomes of the LSV test showing different overpotentials at 10 mV cm^{-2} for the prepared electrodes in 1 M KOH solution for different electrodeposition: (b) currents of −0.75, −1, −1.5, −2, −3, −4, −5 mA for 150 s; (c) duration of 10, 40, 60, 90 and 150 s at −4 mA of the Ni_4Cu_1 particles.

−5 mA during 150 s). The Benchmark response of different prepared electrodes toward HER in 1 M KOH was compared (Fig. 3b). We can notice that the overpotential values decrease with the increase of electrodeposited nickel–copper particles until −4 mA (−99 mV at η_{10}). The additional mass growth of nickel–copper leads to an elevation of the overpotential, indicating that an excess of nickel–copper amount can negatively affect the electrocatalyst by decreasing the number of its active sites.[47]

The effect of the electrodeposition time of Ni_4Cu_1 particles was investigated. For this purpose, we performed LSV tests in 1 M KOH at −4 mA, varying the durations from 10 to 150 s. Increasing the deposition duration decreased the overpotential, reaching an optimal value of −70 mV at 10 mA cm^{-2} for 90 s (Fig. 3c). This is probably due to the enhancement of the active surface area and the presence of coordination sites available for HER at the interface Ni–Cu, as mentioned in previous reports.[48] However, higher time did not produce any additional gains. As mentioned above, an excessive amount of nickel–copper particles can negatively affect the electrocatalyst by decreasing the number of its active sites.[47,49] As far as we are aware, this value was recorded for the first time using a transition metal reinforced by a layer of *para*-phenylenediamine. The free amine group present in the *p*PD plays an important role in the catalyst's performance enhancement, especially by facilitating the electrode/electrolyte interaction. Moreover, amines can influence the selectivity of reactions by favoring specific reaction pathways, which decreases the activation energy required for HER. Integrating the amine groups into the structure of the catalysts improves not only the activity but also the stability and durability, as recently reported when using multiwalled carbon nanotubes doped with nitrogen as a metal-free electrocatalyst. It has also been suggested that amine-based COF combined with Pt could facilitate proton transfer and hydrogen molecule formation.[27,50] Fig. S5a† shows the electrodeposition of *p*PD on the CPE electrode at a constant potential of 0 V *vs.* Ag/AgCl for 40 s. As shown, the current increased during the first few seconds, then it stabilized at a value of −5 μA, indicating that the *p*PD monomer was well deposited on the carbon paste electrode. Once the *p*PD was formed, and in order to incorporate nickel–copper on the surface of the as-prepared electrode *p*PD/CPE, the electrode was promptly and carefully washed with bi-distilled water and placed in the appropriate solution (0.2 M $NiCl_2$–0.05 M $CuCl_2$ in 0.5 M KCl). Fig. S5b† shows the chronopotentiometry curve of Ni–Cu particle deposition (−4 mA for 90 s). The first plot decreases rapidly to a more negative value from −0.3 to −1.2 V *vs.* Ag/AgCl due to the reduction of nickel–copper cations. The potential stabilizes after 10 s at −1.2 (V *vs.* Ag/AgCl), reaching a plateau, which is in agreement with the results of previous studies.[35,51] The prepared electrocatalyst was named Ni_4Cu_1/*p*PD/CPE.

Characterization of the Ni_4Cu_1/*p*PD/CPE electrocatalyst

X-ray diffraction. The crystalline phase of the prepared Ni_4Cu_1/*p*PD/CPE electrocatalyst was characterized using XRD and the results are shown in Fig. 4. The intense peak that appeared at diffraction angle (2θ) of 26.37° and 54.5°, was indexed to the hexagonal structure of the carbon graphite's (002) and (400) planes contained at the surface of the electrode (ICDD 00-041-1487), respectively.[52] The peaks at $2\theta = 36.4°$, 40.28° and 77.33° match the crystal planes (111), (200) and (222) of the cubic structure of copper oxide Cu_2O (ICDD 01-078-2076),[53,54] respectively. The presence of Cu_2O can be explained by the neutral medium of the solution prepared for depositing the nickel–copper particles (0.5 M KCl). The presence of the cubic structure of the nickel metal was indicated by the distinct peak located at $2\theta = 44.35°$, assigned to the (111) plane (ICDD 01-089-7128).[55–57] The peaks at $2\theta = 42.2°$ and 49.9° correspond to (111) and (002) crystalline planes of the cubic structure of the copper metallic (COD 96-410-5682).[58,59] No additional secondary or amorphous phases were identified.

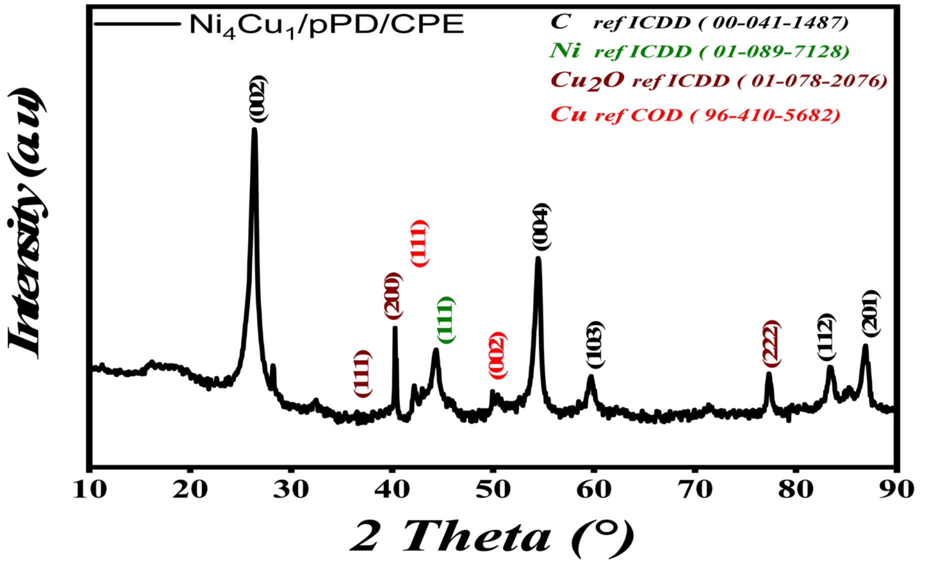

Fig. 4 XRD patterns of the Ni_4Cu_1/*p*PD/CPE electrocatalyst.

Surface morphology and elemental analysis. In order to get a clear understanding of the surface of our prepared electrocatalysts, the composition and microstructural properties were examined using Scanning Electron Microscopy (SEM). As illustrated in Fig. 5, the SEM micrographs of the prepared electrocatalysts Ni_4Cu_1/CPE (Fig. 5a) reveal a homogeneous distribution of lamellae-like structure on their surface, with the presence of a few cracks due to the hydrogen bubbles during the nickel–copper particles deposition. The observed crystalline features are attributed to residual salts such as Cl, most likely from the bath containing 0.2 M $NiCl_2$–0.05 M $CuCl_2$ in 0.5 M KCl. This result is further supported by the presence of Cl in the EDS spectra. At the same time, the existence of *p*PD at the surface of the electrocatalyst Ni_4Cu_1/*p*PD/CPE (Fig. 5b and c) acts as a substrate to allow the homogeneous growth of nickel–copper and prevent the aggregation of nanoparticles on the electrode surface. The presence of filament structures provides a large surface area, resulting in more edge active sites, which play a significant role in the improvement of the electrochemical performance of HER.

An energy-dispersive X-ray (EDX) detector coupled to FEG-SEM and elemental mapping analysis was employed to identify the composition and distribution of element species in the prepared catalyst (Fig. 5d and e). The EDX analysis of the prepared electrocatalyst Ni_4Cu_1/*p*PD/CPE (Fig. 5e) revealed the presence of N, Ni and Cu at the surface of the electrocatalyst. The elemental atom percentages of the sample are illustrated as an inset table in Fig. 5e, which indicates that more nickel is deposited at the electrode surface compared to copper and nitrogen. This elemental mapping image (Fig. 5d) demonstrates the homogenous distribution of the deposited species.

TEM images of the optimized electrode Ni_4Cu_1/*p*PD/CPE are shown in Fig. 6. In agreement with XRD, the images (Fig. 6a and b) show a cluster of overlapping nanostructures with a relatively high contrast, suggesting denser or thicker materials. Some elongated, rod- or needle-like features are visible. The dark, elongated particles correspond to metallic nickel or copper nanoparticles. The high-aspect-ratio features are likely nanorods or nanoneedles, which could be Cu_2O crystals due to their crystalline growth habits. The images (Fig. 6c and d) show well-defined rod- or platelet-like structures clustered in a roughly parallel fashion. These smaller features may correspond to Cu_2O nanocrystals, which tend to form such elongated crystalline domains. The surrounding matrix might be a thin film or support of CPE/*p*PD, given the faint background.

Electrocatalytic performance of electrocatalysts on HER. The electrocatalytic performance of different prepared catalysts *p*PD/CPE, Ni_4Cu_1/CPE, $Ni_4Cu_{1/CPE}$/*p*PD/CPE, for hydrogen production was tested in 1 M KOH solution using a three-electrode system (CPE as Working electrode, platinum wire and Ag/AgCl as auxiliary electrode and reference electrode, respectively). As illustrated in Fig. 7a, the Ni_4Cu_1/*p*PD/CPE electrocatalyst exhibited the highest electrocatalytic activity compared with the other prepared electrocatalysts, with a remarkable overpotential of −70 mV at η_{10}. On Ni_4Cu_1/CPE and *p*PD/CPE electrocatalysts, the obtained overpotential η_{10}

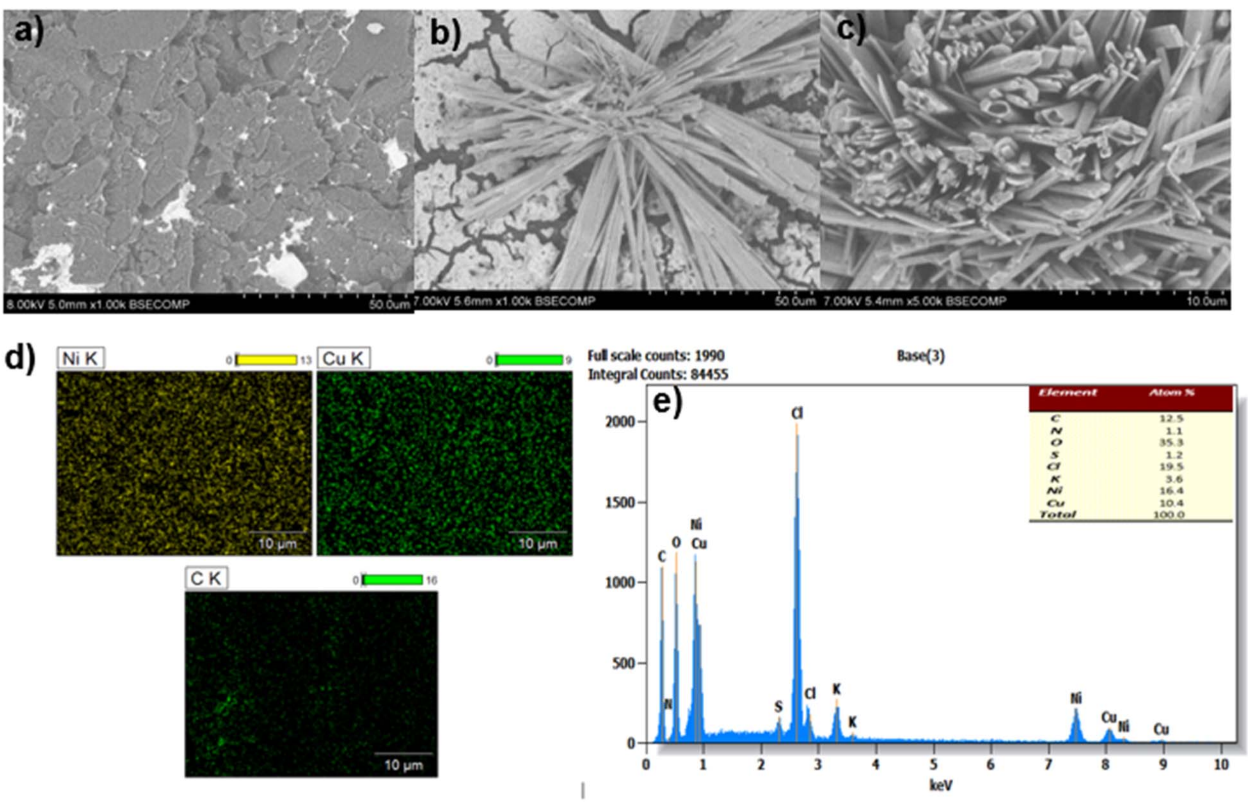

Fig. 5 SEM images of the prepared electrocatalyst. (a) Ni_4Cu_1/CPE and (b and c) Ni_4Cu_1/*p*PD/CPE. (d) EDX pattern of the Ni_4Cu_1/*p*PD/CPE electrocatalyst. (e) EDX mapping of the prepared Ni_4Cu_1/*p*PD/CPE electrocatalyst.

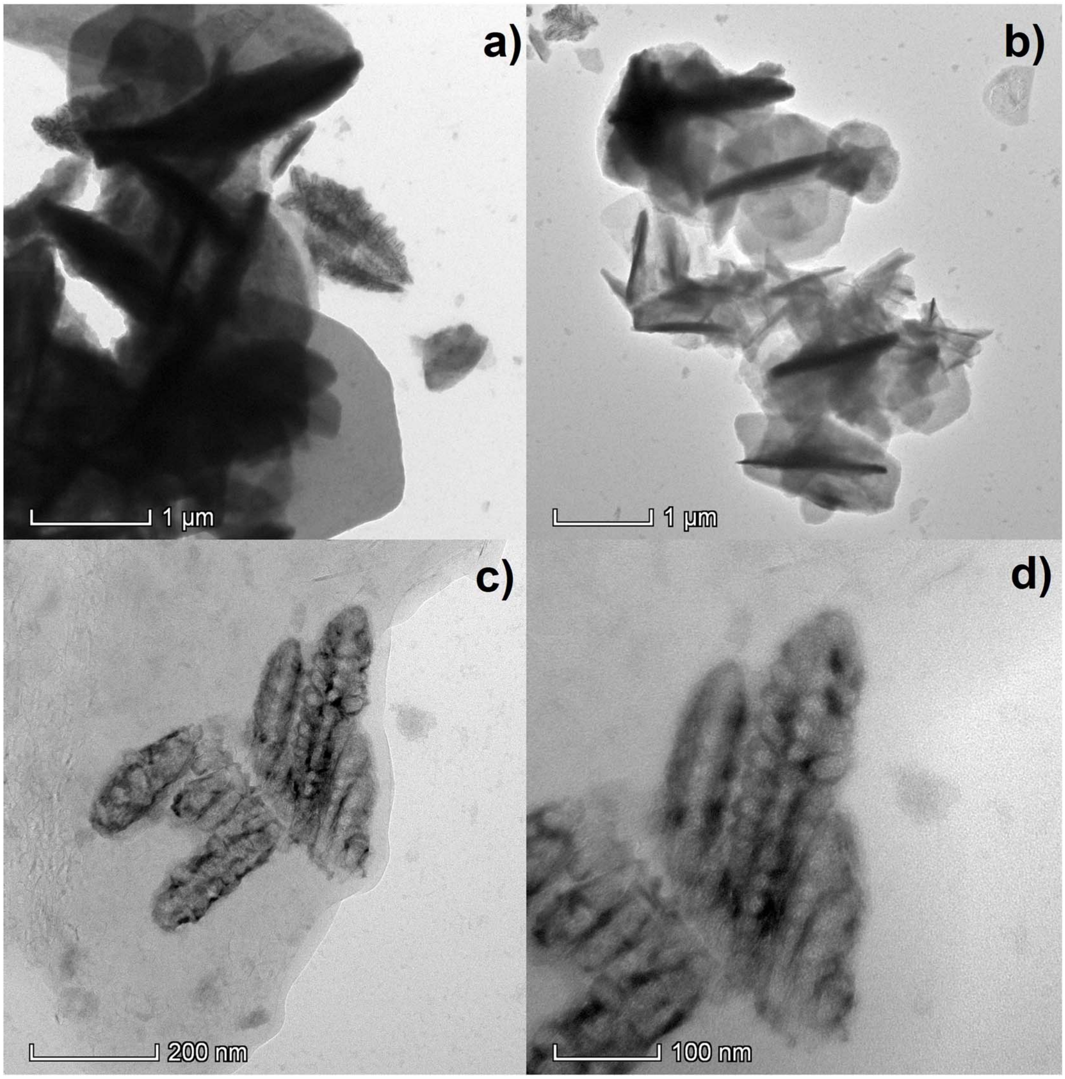

Fig. 6 TEM images of the prepared Ni_4Cu_1/*p*PD/CPE electrocatalyst.

was −171 mV and −657 mV, respectively. Therefore, the combination of *para*-phenylenediamine and Ni_4Cu_1 particles enhanced the HER activity of the CPE electrode, resulting in a shift in overpotential. This phenomenon has been reported earlier by many authors when they investigate the oxidation of alcohol. The existence of *p*PD avoids the agglomeration of the metallic nanoparticles.[23,39] As mentioned earlier, the Tafel slope extracted from the LSV curves was estimated using the Tafel formula $\eta = b\log(j) + a$ (η, b and j are the overpotential, Tafel slope and the current density, respectively).[60,61] A Tafel slope inferior to 40 mV dec^{-1} suggests facile water dissociation and hydrogen production *via* the Volmer–Tafel mechanism, whereas a Tafel slope between 40 and 120 mV dec^{-1} suggests fast reaction kinetics, indicating the Volmer–Heyrovsky mechanism. A Tafel slope superior to 120 mV dec^{-1} indicates slow reaction kinetics and slow water dissociation.[62] The Tafel slopes for Ni_4Cu_1/*p*PD/CPE, and Ni_4Cu_1/CPE were 87, and 85 mV dec^{-1}, respectively, indicating faster reaction kinetics compared to *p*PD/CPE (168 mV dec^{-1}) (Fig. 7b), the higher Tafel slope for Ni_4Cu_1/*p*PD/CPE compared to Ni_4Cu_1/CPE (2 mV dec^{-1}) might be related to higher activation energy and the adsorption characteristic of the intermediates. These smaller Tafel slopes suggest the Volmer–Heyrovsky mechanism, as the slopes are inferior to 120 mV dec^{-1}, indicating fast adsorbed hydrogen formation followed by the reduction of hydrogen cations on the electrode followed by the discharge of the H_{ads} with an electron and water molecule (another hydrogen source) present on the electrode surface, allowing the formation of the hydrogen gas (H_2).[6] The values of the Tafel slope and recorded overpotential for the previously reported electrocatalysts for HER are compared with the values obtained by the Ni_4Cu_1/*p*PD/CPE electrocatalyst Table 1. The electrocatalytic performance of our catalyst was higher than many reported catalysts, such as $NiTe_2$ nanoflakes/Ni foam and NiSe/Ni foam.

Electrochemical impedance measurements were performed on the prepared electrocatalysts (Ni_4Cu_1/*p*PD/CPE, Ni_4Cu_1/CPE, *p*PD/CPE, CPE) to examine the electrochemical behavior at the electrode–solution interface. The measurements were

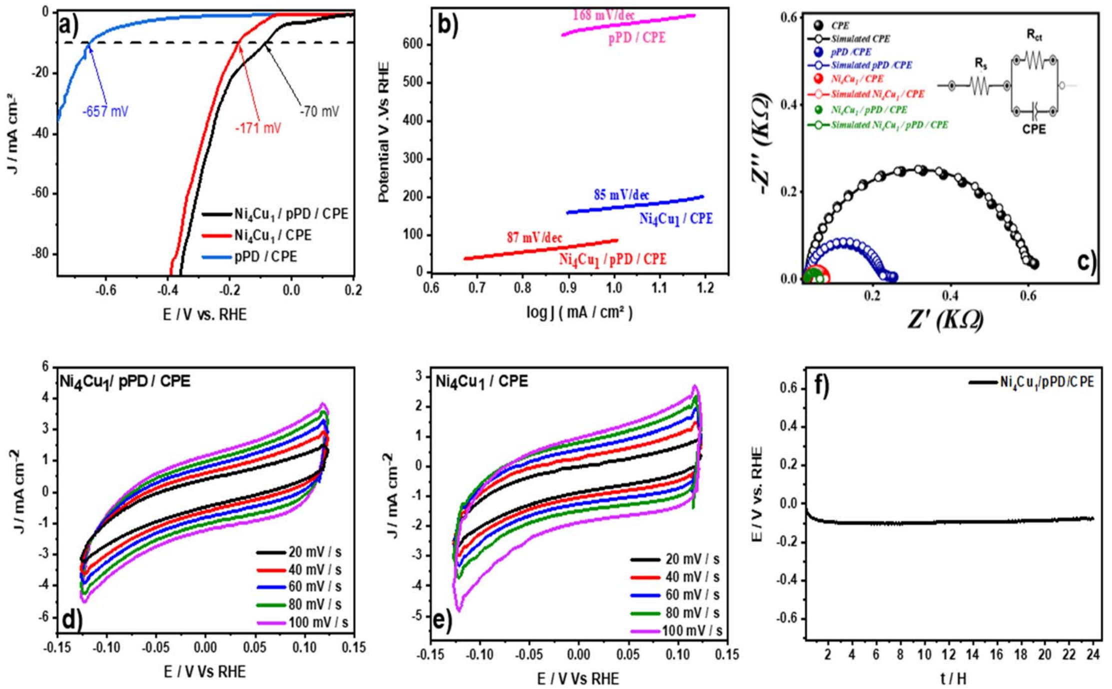

Fig. 7 (a) HER polarization curve, (b) Tafel slope of *p*PD/CPE, Ni_4Cu_1/*p*PD/CPE, and Ni_4Cu_1/CPE. (c) EIS spectra of Ni_4Cu_1/*p*PD/CPE, Ni_4Cu_1/CPE, *p*PD/CPE, and CPE measured at $E = -150$ mV *vs.* RHE, with an amplitude of 0.01 V in 1 M KOH. CV diagrams of (d) Ni_4Cu_1/*p*PD/CPE and (e) Ni_4Cu_1/CPE electrocatalyst in 1 M KOH at scan rates 20–100 mV s^{-1} (f) Continuous water electrolysis chronopotentiometry curves of the Ni_4Cu_1/*p*PD/CPE electrocatalyst at -10 mA cm^{-2} in alkaline media 1 M KOH.

performed in 1 M KOH at a frequency range between 100 kHz–0.1 Hz, a potential amplitude of 0.01 V and an applied potential of -0.15 V *vs.* RHE to calculate the charge transfer resistance (R_{ct}), which is a crucial parameter to evaluate the catalytic reaction's kinetics.[68,69] Fig. 7c displays the findings obtained using the prepared electrocatalysts Ni_4Cu_1/*p*PD/CPE, Ni_4Cu_1/CPE, *p*PD/CPE, and CPE, where the semicircle in the low-frequency area represents the kinetics of HER. The smaller the radius of the semicircle, the higher the electrocatalyst conductivity, and the higher the electron transfer.[70,71] According to Fig. 7c, the prepared electrocatalyst Ni_4Cu_1/*p*PD/CPE shows a smaller radius compared to other prepared electrocatalysts (Ni_4Cu_1/CPE, *p*PD/CPE, CPE), indicating a rapid hydrogen evolution reaction kinetics. The improvement in the electron transfer rate is attributed to a good synergetic impact between Ni_4Cu_1 particles and the *p*PD, which provides a high surface area and good electrical properties, facilitating electron transport.[72–74] The fitting circuit is shown in the inset of Fig. 7c, where R_s represents the electrolyte resistance, R_{ct} represents the charge transfer resistance, and CPE is used as a constant phase element to replace the double-layer capacitor of the charge transfer process. The R_{ct} reached the lowest value with the Ni_4Cu_1/*p*PD/CPE electrocatalyst (33 and 11 Ω), while R_{ct} for Ni_4Cu_1/CPE, *p*PD/CPE, and CPE were 45, 91, 197, 570, and 5 Ω, respectively. The EIS response confirms the HER results obtained from polarization tests (LSV).

In addition, the double layer capacitance C_{dl} method was used to determine the electrochemically active surface area ECSA of the prepared electrocatalysts. The CV curves at different scan rates of (d) Ni_4Cu_1/*p*PD/CPE electrocatalyst and (e) Ni_4Cu_1/CPE electrocatalyst are shown in Fig. 7d and e. The non-faradic potential range was used to examine CV curves, as well as the cathodic current density J_c and the anodic current density J_a to

Table 1 Comparison of the reported HER activities of nickel- and copper-based electrocatalysts with that reported in this work

Catalyst	Overpotential η_{10} (mV *vs.* RHE)	Tafel slope mV dec^{-1}	Reference
$NiTe_2$ nanoflakes/Ni foam	−157	91	63
NiTe nanorods/Ni foam	−202	185	64
Cu nanodots@Ni_3S_2	−128	76.2	65
NiS_2	−454	128	66
Ni_3S_2	−335	97	66
NiSe/Ni foam	−137	118	67
Ni_4Cu_1/*p*PD/CPE	−70	87	Our work

calculate the double-layer capacitance using the following expressions:[75]

$$J_{\mathrm{dl}} = \frac{|J_{\mathrm{c}}| + |J_{\mathrm{a}}|}{2}$$

$$J_{\mathrm{dl}} = C_{\mathrm{dl}} \frac{\mathrm{d}E}{\mathrm{d}t}$$

The value of C_{dl} is 14.23 mF cm^{-2} and 12.15 mF cm^{-2} for the Ni_4Cu_1/*p*PD/CPE and Ni_4Cu_1/CPE electrocatalysts, respectively (Fig. S6†). The ECSA was estimated using the following formula:[76]

$$\mathrm{ECSA} = A_{\mathrm{geometric}} \times \frac{C_{\mathrm{dl}}}{20\ \mu\mathrm{F\ cm}^{-2}}$$

where $A_{\mathrm{geometric}}$ represents the geometric area of the electrocatalyst (00 706 cm^2), and 20 μF cm^{-2} is the ideal double-layer capacitance value.[77] The calculated ECSA values for the prepared electrocatalysts Ni_4Cu_1/*p*PD/CPE and Ni_4Cu_1/CPE are 50.23 cm^2 and 42.89 cm^2, respectively. Consequently, the prepared electrocatalyst has a large effective surface area and high overall conductivity, leading to an enhancement of catalytic performance.[78,79]

Durability and stability are important parameters for assessing the quality of the prepared electrocatalysts.[80] To this end, we used chronopotentiometry and linear voltammetry to investigate the stability of the prepared electrocatalyst Ni_4Cu_1/*p*PD/CPE at −10 mA cm^{-2} in alkaline media, 1 M KOH. As shown in Fig. 7f, the continuous chronopotentiometry curve did not show any movement in the negative direction during the continuous electrolysis, and the overpotential shifted slightly towards the positive direction within 24 h. This confirms that the Ni_4Cu_1/*p*PD/CPE electrocatalyst is highly stable during long-term electrolysis and maintains its hydrogen evolution catalytic activity under stable current density conditions. The long-term stability of the Ni_4Cu_1/*p*PD/CPE electrocatalyst was also tested in 1 M KOH by cyclic voltammetry. Fig. S7† shows a comparison of the polarization curve after 1000 cycles by cyclic voltammetry (CV) in a potential region of the linear sweep polarization region. The polarization curve after the CV test shifted slightly to a negative value, reaching a value of −105 mV at η_{10}. We can notice that for higher current density (100 mA cm^{-2}), only a difference of 10 mV was observed. These comparisons highlight the high performance of the optimized Ni_4Cu_1/*p*PD/CPE electrocatalyst composition.

Conclusion

A novel and highly efficient hybrid electrocatalyst based on Ni–Cu reinforced with a layer of *p*PD was successfully synthesized using a straightforward and rapid electrodeposition method for monitoring the HER in alkaline media. Three electrodepositions modes of *p*PD have been investigated: galvanostatic mode, potentiostatic mode and cyclic voltammetry. The electrodeposition of nickel–copper particles was performed using the galvanostatic mode. The estimated time for catalyst fabrication was 2 to 3 minutes, given a rapid and efficient pathway to the synthesis of electrocatalysts. The best response in terms of overpotential was obtained by *p*PD deposition at 0 V *vs.* Ag/AgCl for 40 s, followed by deposition of Ni–Cu particles at −4 mA for 90 s. The presence of amino groups at the electrode-solution interface with negative charge at 0 V appears to promote uniform dispersion of Ni–Cu particles, preventing their agglomeration. The ESCA calculation and the EIS show that the prepared electrocatalyst has a high surface area and low charge transfer resistance compared to other catalysts, Ni_4Cu_1/CPE and *p*PD/CPE. Interestingly, the Ni_4Cu_1/*p*PD/CPE electrocatalyst demonstrated an excellent catalytic performance for HER, exhibiting a very low overpotential η_{10} of −70 mV. Moreover, it maintained high stability and durability for 24 h in alkaline media. These findings highlight the superior electrocatalytic properties of the Ni_4Cu_1/*p*PD/CPE electrocatalyst for efficient HER activity in water splitting, indicating its promising potential for sustainable H_2 production.

Abbreviations

HER	Hydrogen Evolution Reaction
OER	Oxygen Evolution Reaction
Ni–Cu particles	Nickel–Copper particles
Ni	Nickel
Cu	Copper
CPE	Carbon Paste Electrode
*p*PD	*para*-Phenylenediamine
P*p*PD	Poly-*para*-Phenylenediamine
Ni_4Cu_1/*p*PD/CPE	The prepared electrocatalyst by Ni–Cu particles supported by *p*PD
FE-SEM	Field Emission coupled with Scanning Electron Microscopy
SEM	Scanning Electron Microscopy
EDX	Energy-dispersive X-ray
XRD	X-ray Diffraction
LSV	Linear Sweep Voltammetry
CV	Cyclic Voltammetry
CA	Chronoamperometry
CP	Chronopotentiometry
η_{10}	The overpotential required for an electrocatalyst to reach 10 mA cm^{-2}
RES	Renewable Energy Sources
DC	Direct Current
RHE	Reversible Hydrogen Electrode
Ag/AgCl	Silver Chloride Electrode
WE	Working Electrode
RE	Reference Electrode
CE	Counter Electrode or auxiliary electrode

Data availability

Data ESI† of this study can be found within the article.

Author contributions

Skakri Soufiane: writing – review and editing, writing – original draft, methodology, investigation, data curation, and conceptualization. El Attar Anas: review and editing and conceptualization. Benhaiba Saad: conceptualization. Bouljoihel Badr: data curation. Mouakkar Anas: investigation. Aaddane Abdellah: co-supervision. Adiba Rais: data curation. El Rhazi Mama: writing – review and editing, methodology, data curation, conceptualization, supervision, and funding acquisition.

Conflicts of interest

The authors declare that they have no conflicts of interest.

Acknowledgements

The authors thank the Centre Nationale pour la Recherche Scientifique et Technique (CNRST), especially Mr El Bouji Mohamed, Mr Nejmi Youssef, and Mr Bouchaqour Zakaria for the SEM and TEM facilities.

References

1 F. Dawood, M. Anda and G. M. Shafiullah, Hydrogen production for energy: An overview, *Int. J. Hydrogen Energy*, 2020, **45**, 3847–3869.
2 S. P. Filippov and A. B. Yaroslavtsev, Hydrogen energy: development prospects and materials, *Russ. Chem. Rev.*, 2021, **90**, 627–643.
3 M. Nemiwal, V. Gosu, T. C. Zhang and D. Kumar, Metal organic frameworks as electrocatalysts: Hydrogen evolution reactions and overall water splitting, *Int. J. Hydrogen Energy*, 2021, **46**, 10216–10238.
4 M. Cai, L. Xu, J. Guo, X. Yang, X. He and P. Hu, Recent advances in metal-free electrocatalysts for the hydrogen evolution reaction, *J. Mater. Chem. A*, 2024, **12**, 592–612.
5 A. Lasia, in *Handbook of Fuel Cells*, ed. W. Vielstich, A. Lamm, H. A. Gasteiger and H. Yokokawa, Wiley, 1st edn, 2010.
6 F. Bao, E. Kemppainen, I. Dorbandt, R. Bors, F. Xi, R. Schlatmann, R. Van De Krol and S. Calnan, Understanding the Hydrogen Evolution Reaction Kinetics of Electrodeposited Nickel-Molybdenum in Acidic, Near-Neutral, and Alkaline Conditions, *Chemelectrochem*, 2021, **8**, 195–208.
7 X. Zou and Y. Zhang, Noble Metal-Free Hydrogen Evolution Catalysts for Water Splitting, *Chem. Soc. Rev.*, 2015, **44**, 5148–5180.
8 M. Schalenbach, O. Kasian, M. Ledendecker, F. D. Speck, A. M. Mingers, K. J. J. Mayrhofer and S. Cherevko, The Electrochemical Dissolution of Noble Metals in Alkaline Media, *Electrocatalysis*, 2018, **9**, 153–161.
9 S. Muthu, M. B. Gandhi, S. Saravanan, S. Sekar, S. Arun Kumar, P. Ilanchezhiyan, S. Lee and M. B. Sridharan, Hierarchical nanocomposite of cobalt sulfide nanoflakes-decorated reduced graphene oxide for enhancing the electrocatalytic hydrogen evolution reaction, *Int. J. Hydrogen Energy*, 2024, **52**, 1405–1414.
10 R. Manikandan, S. Sadhasivam, S. Lee, S.-C. Chang, K. Ashok Kumar, C. Bathula, V. Gopalan Sree, D. Young Kim and S. Sekar, Deep eutectic solvents assisted synthesis of AC-decorated NiO nanocomposites for hydrogen evolution reaction, *J. Mol. Liq.*, 2023, **375**, 121338.
11 H. Zhou, D. Zhang, W. Dong, C. Zhou, T. Jiang, Y. Liu, C. Tian, Y. Liu, Y. Liu and B. Mao, Stainless steel mesh-based CoSe/Ni3Se4 heterostructure for efficient electrocatalytic overall water splitting, *Int. J. Hydrogen Energy*, 2023, **48**, 14554–14564.
12 R. Zahra, E. Pervaiz, M. Yang, O. Rabi, Z. Saleem, M. Ali and S. Farrukh, A review on nickel cobalt sulphide and their hybrids: Earth abundant, pH stable electro-catalyst for hydrogen evolution reaction, *Int. J. Hydrogen Energy*, 2020, **45**, 24518–24543.
13 M. Zhang, D. Hu, Z. Xu, B. Liu, M. Boubeche, Z. Chen, Y. Wang, H. Luo and K. Yan, Facile synthesis of Ni-, Co-, Cu-metal organic frameworks electrocatalyst boosting for hydrogen evolution reaction, *J. Mater. Sci. Technol.*, 2021, **72**, 172–179.
14 Z. Li, C. Yu, Y. Wen, Y. Gao, X. Xing, Z. Wei, H. Sun, Y.-W. Zhang and W. Song, Mesoporous Hollow Cu–Ni Alloy Nanocage from Core–Shell Cu@Ni Nanocube for Efficient Hydrogen Evolution Reaction, *ACS Catal.*, 2019, **9**, 5084–5095.
15 B. Hüner, N. Demir and M. F. Kaya, Electrodeposition of NiCu bimetal on 3D printed electrodes for hydrogen evolution reactions in alkaline media, *Int. J. Hydrogen Energy*, 2022, **47**, 12136–12146.
16 S. Mojabi and S. Sanjabi, Decorated fractal Ni-Cu foam with Pd nanoparticles as a high-performance electrocatalyst toward hydrogen evolution reaction, *Thin Solid Films*, 2022, **758**, 139415.
17 H. Ashassi-Sorkhabi, A. Kazempour, S. Moradi-Alavian, E. Asghari and J. J. Lamb, 3D nanostructured nickel film supported to a conducting polymer as an electrocatalyst with exceptional properties for hydrogen evolution reaction, *Int. J. Hydrogen Energy*, 2023, **48**, 29865–29876.
18 S. Cogal, G. Celik Cogal, M. Mičušík, M. Kotlár and M. Omastová, Cobalt-doped WSe2@conducting polymer nanostructures as bifunctional electrocatalysts for overall water splitting, *Int. J. Hydrogen Energy*, 2024, **49**, 689–700.
19 K. E. Ramohlola, K. D. Modibane, M. M. Ndipingwi and E. I. Iwuoha, Polyaniline-based electrocatalysts for electrochemical hydrogen evolution reaction, *Eur. Polym. J.*, 2024, **213**, 113125.
20 R. Zahra, N. Drissi and A. Kumar, Enhanced HER activity through FeAlO3 perovskite oxide incorporated with conducting polymer PANI, *Inorg. Chem. Commun.*, 2024, 113609.
21 N. M. Ivanova, E. A. Soboleva and Y. A. Visurkhanova, Bimetallic Co–Cu polyaniline composites: Structure and electrocatalytic activity, *Russ. J. Appl. Chem.*, 2016, **89**, 1072–1081.

22 P. Pattanayak, N. Pramanik, P. Kumar and P. P. Kundu, Fabrication of cost-effective non-noble metal supported on conducting polymer composite such as copper/polypyrrole graphene oxide (Cu 2 O/PPy–GO) as an anode catalyst for methanol oxidation in DMFC, *Int. J. Hydrogen Energy*, 2018, **43**, 11505–11519.

23 S. Chemchoub, M. Elbasri, El. M. Halim and M. El Rhazi, The electrocatalytic oxidation of methanol on a carbon paste electrode modified by poly(para-phenylenediamine) and Nickel particles, *Mater. Today: Proc.*, 2019, **13**, 720–729.

24 P. Gajendran and R. Saraswathi, Electrocatalytic performance of poly(o-phenylenediamine)-Pt–Ru nanocomposite for methanol oxidation, *J. Solid State Electrochem.*, 2013, **17**, 2741–2747.

25 Z. Nodehi, A. A. Rafati and A. Ghaffarinejad, Palladium-silver polyaniline composite as an efficient catalyst for ethanol oxidation, *Appl. Catal., A*, 2018, **554**, 24–34.

26 Z. Li, X. Dai, K. Du, Y. Ma, M. Liu, H. Sun, X. Ma and X. Zhang, Reduced Graphene Oxide/O-MWCNT Hybrids Functionalized with p-Phenylenediamine as High-Performance MoS_2 Electrocatalyst Support for Hydrogen Evolution Reaction, *J. Phys. Chem. C*, 2016, **120**, 1478–1487.

27 J. H. Park, C. H. Lee, S. Yu, P. Kharel, R. Choi, C. Zhang, P. Y. Huang, J. S.-I. Kwon and H. Yang, Effects of amine-based covalent organic framework on platinum electrocatalyst performance towards hydrogen evolution reaction, *Nano Energy*, 2024, **128**, 109947.

28 X. Ji, L. Bo, Y. Zhang, W. Shi, X. Guan, L. Xia, Y. Shen, Y. Wang and J. Tong, Simply constructed highly dispersed cobalt nanoparticles in diverse N-doped graphitic carbon with remarkable performances for water electrolysis, *Int. J. Hydrogen Energy*, 2022, **47**, 25511–25521.

29 K. Sun, Z. Li, Y. Cao, F. Wang, M. A. Qyyum and N. Han, Recent advancements in perovskite electrocatalysts for clean energy-related applications: Hydrogen production, oxygen electrocatalysis, and nitrogen reduction, *Int. J. Hydrogen Energy*, 2024, **52**, 1104–1126.

30 H. N. Nguyen and D. A. Khuong, in *Engineered Biochar*, ed. S. Ramola, D. Mohan, O. Masek, A. Méndez and T. Tsubota, Springer Nature Singapore, Singapore, 2022, pp. 105–126.

31 F. E. Salih, L. Oularbi, E. Halim, M. Elbasri, A. Ouarzane and M. El Rhazi, Conducting Polymer/Ionic Liquid Composite Modified Carbon Paste Electrode for the Determination of Carbaryl in Real Samples, *Electroanalysis*, 2018, **30**, 1855–1864.

32 L. Oularbi, M. Turmine, F. E. Salih and M. El Rhazi, Ionic liquid/carbon nanofibers/bismuth particles novel hybrid nanocomposite for voltammetric sensing of heavy metals, *J. Environ. Chem. Eng.*, 2020, **8**, 103774.

33 A. El Attar, L. Oularbi, S. Chemchoub and M. El Rhazi, Preparation and characterization of copper oxide particles/polypyrrole (Cu2O/PPy) via electrochemical method: Application in direct ethanol fuel cell, *Int. J. Hydrogen Energy*, 2020, **45**, 8887–8898.

34 Z. Zhang, Y. Wu and D. Zhang, Potentiostatic electrodeposition of cost-effective and efficient Ni–Fe electrocatalysts on Ni foam for the alkaline hydrogen evolution reaction, *Int. J. Hydrogen Energy*, 2022, **47**, 1425–1434.

35 S. Chemchoub, A. El Attar, L. Oularbi, S. A. Younssi, F. Bentiss, C. Jama and M. El Rhazi, Electrosynthesis of eco-friendly electrocatalyst based nickel-copper bimetallic nanoparticles supported on poly-phenylenediamine with highest current density and early ethanol oxidation onset potential, *Int. J. Hydrogen Energy*, 2022, **47**, 39081–39096.

36 Y. Li, K. Dastafkan, Q. Sun, Y. Ma, X. Wang, X. Yang, Z. Wang and C. Zhao, Ni-based 3D hierarchical heterostructures achieved by selective electrodeposition as a bifunctional electrocatalyst for overall water splitting, *Electrochim. Acta*, 2021, **379**, 138042.

37 S. Dongre S, A. Iqbal, R. Thapa, P. M, S. Ramu and R. G. Balakrishna, Synergistic Catalyst Design for Enhanced Electrochemical Hydrogen Evolution: Fe_2O_3/MoS_2/Ti 3 C 2 T *x* MXene Ternary Composite, *ACS Appl. Eng. Mater.*, 2024, **2**, 943–954.

38 A. Kumar and S. Bhattacharyya, Porous NiFe-Oxide Nanocubes as Bifunctional Electrocatalysts for Efficient Water-Splitting, *ACS Appl. Mater. Interfaces*, 2017, **9**, 41906–41915.

39 E. M. Halim, M. Elbasri, H. Perrot, O. Sel, K. Lafdi and M. El Rhazi, Synthesis of carbon nanofibers/poly(para-phenylenediamine)/nickel particles nanocomposite for enhanced methanol electrooxidation, *Int. J. Hydrogen Energy*, 2019, **44**, 24534–24545.

40 A. K. D. Diaw, D. Gningue-Sall, A. Yassar and J. J. Aaron, New poly(p-substituted-N-phenylpyrrole)s. Electrosynthesis, electrochemical properties and characterization, *Synth. Met.*, 2013, **179**, 74–85.

41 L. M. Samyn, R. S. Babu, M. Devendiran and A. L. F. De Barros, Electropolymerization of p-phenylenediamine films on carbon fiber fabrics electrode for flexible supercapacitors: surface and electrochemical characterizations, *Ionics*, 2020, **26**, 3041–3050.

42 E. M. Halim, H. Perrot, O. Sel, C. Debiemme-Chouvy, K. Lafdi and M. El Rhazi, Electrosynthesis of hierarchical Cu2O–Cu(OH)2 nanodendrites supported on carbon nanofibers/poly(para-phenylenediamine) nanocomposite as high-efficiency catalysts for methanol electrooxidation, *Int. J. Hydrogen Energy*, 2021, **46**, 19926–19938.

43 X. Qiao, H. Li, W. Zhao and D. Li, Effects of deposition temperature on electrodeposition of zinc–nickel alloy coatings, *Electrochim. Acta*, 2013, **89**, 771–777.

44 Y. Li, X. Xie, Y. Wang, X. Yuan and F. Li, Nickel-based alloy nanoparticles anchored on nickel mesh towards excellent and sustainable water electrolysis, *Int. J. Electrochem. Sci.*, 2023, **18**, 100216.

45 S. Chemchoub, A. El Attar, L. Oularbi, S. A. Younssi, F. Bentiss, C. Jama and M. El Rhazi, Electrosynthesis of eco-friendly electrocatalyst based nickel-copper bimetallic nanoparticles supported on poly-phenylenediamine with highest current density and early ethanol oxidation onset potential, *Int. J. Hydrogen Energy*, 2022, **47**, 39081–39096.

46 W. Li, J. Hao, S. Mu and W. Liu, Electrochemical behavior and electrodeposition of Ni-Co alloy from choline chloride-

ethylene glycol deep eutectic solvent, *Appl. Surf. Sci.*, 2020, **507**, 144889.

47 H. Zhu, J. Wang, X. Liu and X. Zhu, Three-dimensional porous graphene supported Ni nanoparticles with enhanced catalytic performance for Methanol electrooxidation, *Int. J. Hydrogen Energy*, 2017, **42**, 11206–11214.

48 A. Irshad and N. Munichandraiah, Electrodeposited Nickel–Cobalt–Sulfide Catalyst for the Hydrogen Evolution Reaction, *ACS Appl. Mater. Interfaces*, 2017, **9**, 19746–19755.

49 W. Tan, X. Liu, W. Liu, H. He and Y. Yang, Galvanostatic electrodeposition of a self-supported Ni–Se–Lu/NF electrocatalyst for efficient alkaline hydrogen evolution reaction, *Int. J. Hydrogen Energy*, 2024, **80**, 270–279.

50 R. P. Dighole, A. V. Munde, B. B. Mulik, S. C. Dhawale and B. R. Sathe, Facile synthesis of nitrogen-containing multiwalled carbon nanotubes as a worth metal-free electrocatalyst for hydrogen evolution reaction and semicarbazide oxidation, *Int. J. Hydrogen Energy*, 2024, **91**, 285–293.

51 N. A. M. Barakat, M. A. Yassin, F. S. Al-Mubaddel and M. T. Amen, New electrooxidation characteristic for Ni-based electrodes for wide application in methanol fuel cells, *Appl. Catal., A*, 2018, **555**, 148–154.

52 F. M. Souza, P. Böhnstedt, V. S. Pinheiro, L. A. Oliveira, B. L. Batista, L. S. Parreira, R. A. Antunes and M. C. Santos, Niobium increasing the electrocatalytic activity of palladium for alkaline direct ethanol fuel cell, *J. Electroanal. Chem.*, 2020, **858**, 113824.

53 X. Chen, R. Chen, X. Zhu, Q. Liao, Y. Zhang, D. Ye, B. Zhang, Y. Yu and J. Li, A solar responsive cubic nanosized CuS/Cu2O/Cu photocathode with enhanced photoelectrochemical activity, *J. Catal.*, 2019, **372**, 182–192.

54 A. El Attar, L. Oularbi, S. Chemchoub and M. El Rhazi, Preparation and characterization of copper oxide particles/polypyrrole (Cu2O/PPy) via electrochemical method: Application in direct ethanol fuel cell, *Int. J. Hydrogen Energy*, 2020, **45**, 8887–8898.

55 C. Cui, Y. Liu, S. Mehdi, H. Wen, B. Zhou, J. Li and B. Li, Enhancing effect of Fe-doping on the activity of nano Ni catalyst towards hydrogen evolution from NH3BH3, *Appl. Catal., B*, 2020, **265**, 118612.

56 X. Wang, S. Yang, Y. Yu, M. Dou, Z. Zhang and F. Wang, Low-loading Pt nanoparticles embedded on Ni, N-doped carbon as superior electrocatalysts for oxygen reduction, *Catal. Sci. Technol.*, 2020, **10**, 65–69.

57 S. A. Al-Thabaiti, Z. Khan and M. A. Malik, Bimetallic Ag-Ni nanoparticles as an effective catalyst for hydrogen generation from hydrolysis of sodium borohydride, *Int. J. Hydrogen Energy*, 2019, **44**, 16452–16466.

58 M. Negem, H. Nady and C. W. Dunnill, Nanocrystalline Ni–Cu Electroplated Alloys Cathodes for Hydrogen Generation in Phosphate-Buffered Neutral Electrolytes, *J. Bio Tribo Corros.*, 2020, **6**, 116.

59 M. Negem and H. Nady, Electroplated Ni-Cu nanocrystalline alloys and their electrocatalytic activity for hydrogen generation using alkaline solutions, *Int. J. Hydrogen Energy*, 2017, **42**, 28386–28396.

60 Y. Zhu, T. Liu, L. Li, S. Song and R. Ding, Nickel-based electrodes as catalysts for hydrogen evolution reaction in alkaline media, *Ionics*, 2018, **24**, 1121–1127.

61 J. Ping, Y. Wang, Q. Lu, B. Chen, J. Chen, Y. Huang, Q. Ma, C. Tan, J. Yang, X. Cao, Z. Wang, J. Wu, Y. Ying and H. Zhang, Self-Assembly of Single-Layer CoAl-Layered Double Hydroxide Nanosheets on 3D Graphene Network Used as Highly Efficient Electrocatalyst for Oxygen Evolution Reaction, *Adv. Mater.*, 2016, **28**, 7640–7645.

62 H. Sun, C. Tian, Y. Li, J. Wu, Q. Wang, Z. Yan, C. Li, F. Cheng and M. Du, Coupling NiCo Alloy and CeO2 to Enhance Electrocatalytic Hydrogen Evolution in Alkaline Solution, *Adv. Sustainable Syst.*, 2020, **4**, 2000122.

63 S. Anantharaj, K. Karthick and S. Kundu, $NiTe_2$ Nanowire Outperforms Pt/C in High-Rate Hydrogen Evolution at Extreme pH Conditions, *Inorg. Chem.*, 2018, **57**, 3082–3096.

64 L. Yang, H. Xu, H. Liu, D. Cheng and D. Cao, Active Site Identification and Evaluation Criteria of In Situ Grown CoTe and NiTe Nanoarrays for Hydrogen Evolution and Oxygen Evolution Reactions, *Small Methods*, 2019, **3**, 1900113.

65 J.-X. Feng, J.-Q. Wu, Y.-X. Tong and G.-R. Li, Efficient Hydrogen Evolution on Cu Nanodots-Decorated Ni3S2 Nanotubes by Optimizing Atomic Hydrogen Adsorption and Desorption, *J. Am. Chem. Soc.*, 2018, **140**, 610–617.

66 N. Jiang, Q. Tang, M. Sheng, B. You, D. Jiang and Y. Sun, Nickel sulfides for electrocatalytic hydrogen evolution under alkaline conditions: a case study of crystalline NiS, NiS2, and Ni3S2 nanoparticles, *Catal. Sci. Technol.*, 2016, **6**, 1077–1084.

67 H. Ren, Z.-H. Huang, Z. Yang, S. Tang, F. Kang and R. Lv, Facile synthesis of free-standing nickel chalcogenide electrodes for overall water splitting, *J. Energy Chem.*, 2017, **26**, 1217–1222.

68 N. Hallemans, W. D. Widanage, X. Zhu, S. Moharana, M. Rashid, A. Hubin and J. Lataire, Operando electrochemical impedance spectroscopy and its application to commercial Li-ion batteries, *J. Power Sources*, 2022, **547**, 232005.

69 L. Oularbi, M. Turmine and M. El Rhazi, Preparation of novel nanocomposite consisting of bismuth particles, polypyrrole and multi-walled carbon nanotubes for simultaneous voltammetric determination of cadmium(II) and lead(II), *Synth. Met.*, 2019, **253**, 1–8.

70 C. Hitz and A. Lasia, Experimental study and modeling of impedance of the her on porous Ni electrodes, *J. Electroanal. Chem.*, 2001, **500**, 213–222.

71 B. Fei, Z. Chen, J. Liu, H. Xu, X. Yan, H. Qing, M. Chen and R. Wu, Ultrathinning Nickel Sulfide with Modulated Electron Density for Efficient Water Splitting, *Adv. Energy Mater.*, 2020, **10**, 2001963.

72 C. R. Rawool, N. S. Punde, A. S. Rajpurohit, S. P. Karna and A. K. Srivastava, High energy density supercapacitive material based on a ternary hybrid nanocomposite of

cobalt hexacyanoferrate/carbon nanofibers/polypyrrole, *Electrochim. Acta*, 2018, **268**, 411–423.

73 Z. Kang, M. Zhao, Y. Wu, T. Xia, J.-P. Cao, W. Cai and L. Chen, Facial fabrication of yolk-shell Pd-Ni-P alloy with mesoporous structure as an advanced catalyst for methanol electro-oxidation, *Appl. Surf. Sci.*, 2019, **484**, 441–445.

74 L. Oularbi, M. Turmine and M. El Rhazi, Electrochemical determination of traces lead ions using a new nanocomposite of polypyrrole/carbon nanofibers, *J. Solid State Electrochem.*, 2017, **21**, 3289–3300.

75 H. Dong, T. Lei, Y. He, N. Xu, B. Huang and C. T. Liu, Electrochemical performance of porous Ni3Al electrodes for hydrogen evolution reaction, *Int. J. Hydrogen Energy*, 2011, **36**, 12112–12120.

76 A. Kellenberger, N. Vaszilcsin, W. Brandl and N. Duteanu, Kinetics of hydrogen evolution reaction on skeleton nickel and nickel–titanium electrodes obtained by thermal arc spraying technique, *Int. J. Hydrogen Energy*, 2007, **32**, 3258–3265.

77 N. Krstajic, V. Jovic, L. Gajickrstajic, B. Jovic, A. Antozzi and G. Martelli, Electrodeposition of Ni–Mo alloy coatings and their characterization as cathodes for hydrogen evolution in sodium hydroxide solution, *Int. J. Hydrogen Energy*, 2008, **33**, 3676–3687.

78 M. A. Lukowski, A. S. Daniel, F. Meng, A. Forticaux, L. Li and S. Jin, Enhanced Hydrogen Evolution Catalysis from Chemically Exfoliated Metallic MoS 2 Nanosheets, *J. Am. Chem. Soc.*, 2013, **135**, 10274–10277.

79 M. Y. Gao, C. Yang, Q. B. Zhang, Y. W. Yu, Y. X. Hua, Y. Li and P. Dong, Electrochemical fabrication of porous Ni-Cu alloy nanosheets with high catalytic activity for hydrogen evolution, *Electrochim. Acta*, 2016, **215**, 609–616.

80 Y. Wei, R. A. Soomro, X. Xie and B. Xu, Design of efficient electrocatalysts for hydrogen evolution reaction based on 2D MXenes, *J. Energy Chem.*, 2021, **55**, 244–255.